Analytical Methods

ROYAL SOCIETY OF CHEMISTRY

PAPER

View Article Online
View Journal | View Issue

Cite this: *Anal. Methods*, 2025, **17**, 9381

Highly efficient Nile red staining for the rapid quantification of microplastic number concentrations using flow cytometry

Yuki Kuruma, *[ab] Hiromu Sakurai [b] and Tomoaki Okuda [a]

Fluorescent staining of microplastics (MPs) with Nile red (NR) improves the sensitivity of optical techniques, including microscopy and flow cytometry (FCM), and is commonly employed to quantify MP number concentrations. However, staining efficiency varies depending on the polymer type and surface characteristics, often resulting in insufficient fluorescence intensity. This study presents an improved protocol using a swelling-mediated NR staining method, which enables NR to be encapsulated within MPs rather than merely adsorbed on the surface, as in conventional methods. This technique yields strongly fluorescent MPs, improving detection sensitivity and allowing identification of MPs smaller than a few micrometers. Using this method in combination with FCM, we successfully quantified MP number concentration for particles with diameters less than 10 μm. The pretreatment and staining procedures were optimized using polystyrene particle suspensions (2, 5, and 10 μm) with known number concentrations. The staining efficiencies were close to 1. Recovery tests were also carried out using simulated environmental samples with tap water as the matrix. After correcting for the FCM's counting efficiency, the recovery rates were 0.993 ± 0.038 (2 μm), 0.988 ± 0.029 (5 μm), and 0.846 ± 0.100 (10 μm). Differences in recovery rates were attributed to instrument-specific counting efficiency, with no evidence of systematic uncertainty associated with the staining process. Our findings indicate the effectiveness of the swelling-mediated NR staining technique for quantifying MPs and highlight its potential as a rapid and reliable approach for analyzing MPs in environmental samples when combined with high-throughput FCM.

Received 4th July 2025
Accepted 1st November 2025

DOI: 10.1039/d5ay01093d

rsc.li/methods

1 Introduction

Microplastics (MPs) are plastic particles smaller than 5 mm and have garnered significant attention due to concerns regarding their environmental impact and potential health effects on humans.[1] Recent studies suggest that MPs released into marine and freshwater environments may be transferred from lower trophic organisms, such as plankton, to higher trophic organisms, such as fish,[2,3] underscoring the urgent need to elucidate their ecological impacts. To address this, various approaches have been undertaken, including quantitative evaluations through sampling and measurement, spatial distribution assessments *via* modeling and simulations, and biological and cellular experiments.[4–7]

Field studies have investigated environmental MPs through field sampling and quantified their size and number concentration. The analysis of MP samples collected from various environmental media—including the ocean, rivers, soil, and atmosphere—requires preliminary concentration procedures, as well as chemical treatments and density separation to remove impurities composed of organic and inorganic matter.[8,9] Measurement methods for MP samples after pre-treatment include imaging techniques for shape and size analysis using microscopes; spectroscopic techniques for material identification using infrared (IR) or Raman spectroscopy, and pyrolysis gas chromatography, which analyzes materials based on the gases produced by the thermal decomposition of MPs.[10,11] Although these measurement techniques are well established, they have limitations in terms of measurable particle size; specifically, the lower detection limit for individual particles is typically greater than 1 μm,[12] making it challenging to quantify MPs smaller than a few micrometers. Furthermore, with microscopic and spectroscopic methods such as IR and Raman, MPs collected on filters or substrates are counted, which requires an adequate number of particles to achieve statistically reliable results and generally involves substantial time and labor. Recently, many novel measurement techniques have been proposed to address shortcomings of conventional methods, particularly those related to particle size limitations and low throughput. Among these, flow cytometry (FCM)[13,14] has

[a]*Department of Applied Chemistry, Faculty of Science and Technology, Keio University, 3-14-1 Hiyoshi, Kohoku-ku, Yokohama, Kanagawa, 223-8522, Japan*

[b]*National Metrology Institute of Japan (NMIJ), National Institute of Advanced Industrial Science and Technology (AIST), 1-1-1 Umezono, Tsukuba, Ibaraki 305-8563, Japan. E-mail: y.kuruma@aist.go.jp*

attracted attention as a promising method for the rapid measurement of MP size and number concentration.

FCM determines the particle size (approximately 100 nm–100 μm) and number concentration of suspended particles by analyzing light scattering and fluorescence as particles or cells pass through a laser-irradiation area in a flow cell. Similar to fluorescence microscopy, fluorescent labeling enables FCM to distinguish MPs from impurity particles based on their fluorescence signals. FCM measures particles in prepared suspensions rather than on filters. For environmental samples, upfront preconcentration is often necessary; however, the measurement itself does not require filter-based collection, unlike fluorescence microscopy or IR/Raman imaging. It can automatically measure particle suspensions within minutes, enabling faster evaluation of MP number concentration compared to conventional methods. In FCM- and microscopy-based MPs measurements, Nile red (NR) staining is frequently used to improve detection sensitivity and to distinguish MPs from non-MP materials through selective labeling.[15,16] NR is a hydrophobic dye with good affinity for various types of MPs and readily adsorbs onto their surfaces. Fluorescence detection using appropriate excitation light and fluorescence filters—such as a blue light ("Crime lite", 450–510 nm) in combination with an orange filter (529 nm)—is feasible.[15] However, while NR fluorescence staining is expected to enhance the sensitivity of optical measurements like FCM and microscopy, the efficiency of NR adsorption onto MPs (*i.e.*, the ease of staining) depends on the polymer type and surface characteristics (chemical functional groups), which can sometimes result in insufficient fluorescence intensity for detection. For example, earlier studies have reported that certain polymer types exhibit low fluorescence intensity, making detection difficult with FCM.[13,17] Efficient fluorescence staining of MPs with NR is therefore crucial for achieving high-sensitivity measurements using optical techniques.

The staining method that uses the swelling phenomenon of polymers is an effective technique.[18] This method is hereafter referred to as the swelling-mediated staining method. The process begins with the preparation of a particle suspension by dispersing MPs in a poor solvent, typically ultrapure water. A small amount of an organic solvent—one that serves as a good solvent for the MPs—is then added, causing the MPs to swell. This swelling enables the penetration of fluorescent dye molecules into the interior of the MPs. The dye is then added to stain the swollen MPs. After staining, the organic solvent is removed using separation techniques such as evaporation and centrifugation, causing the MPs to shrink back to their original size and encapsulate the dyes within. The swelling-mediated staining method yields fluorescent particles with high fluorescence intensity and minimal dye leakage, making it a simple and efficient approach for fluorescent labeling. Previous studies have demonstrated the applicability of this technique for staining polystyrene (PS),[19–23] polymethyl methacrylate,[18] and polypropylene[24] using various organic and inorganic fluorescent dyes, such as NR,[21,25] fluorescein isothiocyanate,[18] tris(2,2′-bipyridyl)ruthenium(II) chloride,[18] and chlorophyll *a*.[20]

Earlier studies have demonstrated the effectiveness of the swelling-mediated staining method; however, accurately determining particle number concentration after staining remains challenging. For example, interference from unreacted dyes can adversely affect number concentration measurements. Unreacted fluorescent dyes often remain in MP suspensions following swelling-mediated staining and can form aggregates that interfere with optical detection. To remove these unreacted dyes, previous studies have employed centrifugation[18,20–22,25] and vacuum filtration.[19,23,24] However, such separation and purification procedures may lead to particle adsorption onto the inner walls of centrifuge tubes or the surfaces of membrane filters, resulting in particle loss. In particular, the recovery rate of MPs from membrane filters is highly dependent on the filter material,[26] introducing considerable uncertainty in the quantification of MP number concentrations. Given the inherent limitations of conventional methods such as centrifugation and vacuum filtration in achieving complete recovery, the direct quantification of fluorescent MP number concentration following swelling-mediated staining remains largely unexplored.

This study presents a fluorescence staining protocol for accurately quantifying MP number concentrations using optical techniques such as FCM. To our knowledge, this is the first report to quantify particle number concentration while explicitly evaluating the effect of residual unreacted dye remaining after the swelling-mediated staining method. Unlike conventional staining methods that rely on the adsorption of NR onto the surface of MPs, the proposed method achieves high-sensitivity fluorescence detection and accurate quantification by using a swelling-mediated staining method. The main difference between the swelling-mediated staining method used in earlier studies and the method used in this work is that we remove the organic solvent by room-temperature evaporation rather than by centrifugation and vacuum filtration. This modification minimizes particle loss during the staining procedure. This paper discusses the optimization of the swelling-mediated staining procedure through a systematic evaluation of experimental conditions. To validate this method, staining efficiencies and recovery rates were assessed using PS particle suspensions with accurately determined number concentrations. Recovery tests were also conducted using simulated environmental samples with tap water as the matrix. The target MP samples for this method are those already collected from environmental media, subjected to necessary pretreatment (including preconcentration, density separation, and chemical digestion), and provided either as aqueous dispersions or powders.

2 Experimental

2.1 Reagents and microplastic particles

2.1.1 PS standard suspension. Spherical PS particles were used as MP samples to evaluate the performance of the proposed method. PS particles with nominal diameters of 2 μm (Cat. no.: 07310-15), 5 μm (Cat. no.: 17135-5), and 10 μm (Cat. no.: 17136-5) were purchased from Polysciences, Inc. The width

of the particle size distribution, expressed as the coefficients of variation, was 3%, 5%, and 10%, respectively. The stock suspensions were aqueous dispersions containing 2.5% solids by mass. Aliquots of these suspensions were diluted with ultrapure water to prepare a "PS standard suspension" with a particle number concentration of 1×10^6 particles mL^{-1}. Prior to use, the PS standard suspensions were redispersed and homogenized by ultrasonication for 2 min, followed by rotary shaking for 10 min.

The particle number concentrations of the PS standard suspensions were accurately calibrated using the mass-measurement-type optical particle counting (M-OPC) method. The M-OPC method is a highly reliable absolute measurement technique for measuring particle number concentrations in liquids, and its details are described in the literature.[27,28] A brief overview is provided below. The particle number concentration is determined by simultaneously measuring the particle count using a liquid-borne particle counter and the suspension mass using an electronic balance. The uncertainty associated with the M-OPC method was thoroughly evaluated, and the resulting particle number concentrations were traceable to the International System of Units (SI). Furthermore, the method's validity was corroborated by comparison with an independent technique—the microscopic counting method—which showed agreement within the range of measurement uncertainty.

2.1.2 Kaolin particles and tap water as simulated environmental samples. A mixture of kaolin particles and tap water was used as a simulated environmental sample. Kaolin particles were used as model particles to represent the insoluble impurities commonly found in environmental samples. Kaolin, a type of clay mineral, is recognized in the Japanese Industrial Standards as a turbidity standard for industrial water testing, where a particle suspension prepared by adding a defined amount of Kaolin to pure water is used as a standard suspension.[29] In this study, a kaolin-based turbidity standard suspension with a turbidity of 100 (Cat. no.: 206-06701, Fujifilm Wako Pure Chemical) was used.

Unlike ultrapure water, tap water contains a more complex chemical composition, including dissolved substances and insoluble fine particles—some of which may originate from water pipes. The tap water used in the experiments was collected from a laboratory faucet.

A simulated environmental sample was prepared by mixing 20 μL of the kaolin turbidity standard solution with 480 μL of tap water. This mixture was employed in the recovery test described in Section 3.7.

2.1.3 Fluorescent dye. NR (Cat. no.: 140-08813, Fujifilm Wako Pure Chemical Corp.) was employed as the fluorescent dye for MPs. Powdered NR was dissolved in tetrahydrofuran (THF) (Cat. no.: 204-08745, Fujifilm Wako Pure Chemical Corp.) to prepare an NR solution at a concentration of 1 mg mL^{-1}. The prepared NR solution was filtered employing a polytetrafluoroethylene (PTFE) syringe filter with a 0.22 μm pore size (Millex-LG, Merck KGaA) to remove impurities.

2.1.4 Surfactant. To improve the dispersion stability of the MP suspensions and suppress NR aggregation, Tween-20 (Cat. no.: 166-21115, Fujifilm Wako Pure Chemical Corp.) was used as the surfactant. Tween-20 was diluted with ultrapure water to prepare a 10% (v/v) aqueous solution. The prepared Tween-20 solution was filtered using a PTFE syringe filter with a 0.22 μm pore size to remove fine particles.

2.2 Nile red staining *via* the swelling procedure

This section explains the specific procedures used in the staining method and FCM measurement. Unless otherwise noted, MPs were stained using the reagent amounts and protocols outlined below, and the resulting samples were used as PS suspensions for FCM measurements. Fig. 1 displays a schematic diagram of the staining procedure. First, 900 μL of a PS standard suspension was transferred into a glass vial, followed by the addition of 100 μL of a 10% Tween-20 aqueous solution. Subsequently, 320 μL of THF was added, and the vial was gently shaken by hand for 5 s to mix, taking care to avoid foaming. Then, 10 μL of a 1 mg mL^{-1} NR solution was added, and the vial was gently shaken again for 5 s. At this stage, the PS particles in the suspension swelled, allowing the NR molecules to diffuse into the internal polymer matrix of the PS.[18,20,24] The vial was left uncapped at room temperature for 14 h to 20 h to allow the THF to evaporate. During this process, the PS particles shrank and returned to their original size, thereby

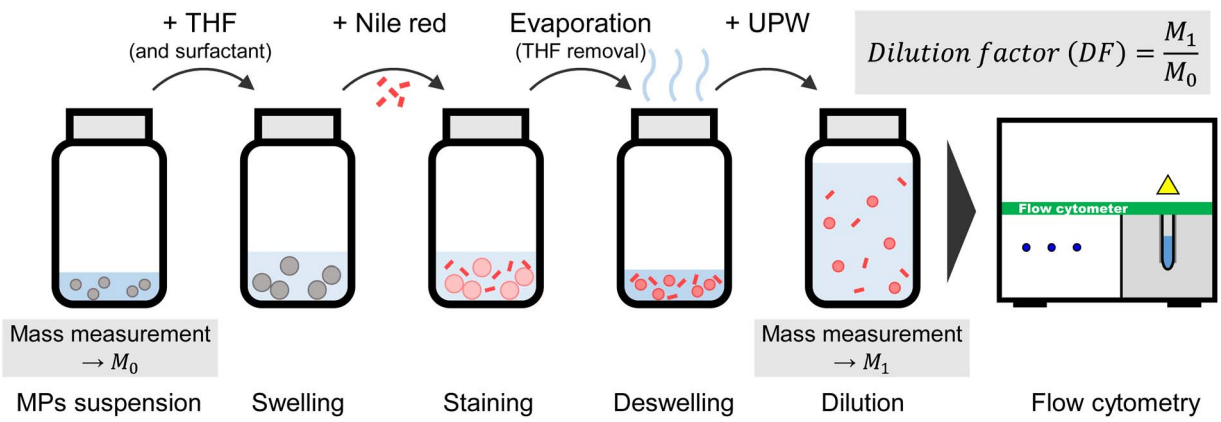

Fig. 1 Schematic diagram of Nile red staining *via* the swelling procedure.

encapsulating the NR molecules within them.[18,20,24] Evaporation resulted in a mass loss of 300–400 mg, consistent with the removal of nearly all of the added THF (320 μL). Following evaporation, 9 mL of ultrapure water was added to the PS suspension for dilution. The sample was subsequently homogenized by vortex mixing for 20 s, ultrasonication for 60 s, and rotary shaking for at least 10 min. The resulting suspension was diluted 11-fold relative to the initial PS standard suspension, yielding a particle number concentration of 0.9×10^5 particles mL^{-1}. The masses of both the added PS standard suspension and final PS suspension were measured using an electronic balance to accurately determine the dilution factor. For the quantitative evaluation of staining efficiency using the swelling-mediated staining method (Sections 3.6 and 3.7), three replicate PS suspensions were prepared for each particle size. Moreover, three blank samples—with no PS standard suspension added—were prepared using the same procedure. For the recovery test using simulated environmental samples (Section 3.7), 400 μL of the PS standard suspension and 500 μL of the simulated environmental sample (see Section 2.1) were used instead of the 900 μL of the PS standard suspension. The same staining procedure was then applied.

2.3 Flow cytometry

The PS suspension samples were prepared according to the procedure described in Section 2.2 and analyzed using an FCM. A CyFlow Space (Sysmex Partec GmbH) was used for the FCM measurements. A blue laser with a wavelength of 488 nm and an output power of 200 mW were used for excitation. Side-scattered (SS) signals detected by the FCM, along with fluorescence (FL) signals filtered through a bandpass filter centered at 520 nm, were acquired and analyzed using a high-speed digitizer (PXI-5122, National Instruments Corp.). The digitizer was controlled by a custom-built LabVIEW program, allowing it to function as a multichannel pulse height analyzer. The pulse height (voltage) of each particle was recorded. The sample flow rate during FCM measurements was set at 1 μL s^{-1}, and both SS and FL signals were acquired over a 30 s measurement period. The total sample volume analyzed per measurement was 30 μL. The particle number concentration was calculated by dividing the number of detected particles by the analyzed sample volume. Each sample was measured in triplicate, and the mean value was presented. Although our experimental setup used SS, forward scattering, which is generally more sensitive to particles size, can also be applicable.

We used a custom-built pulse height analyzer in place of the FCM's built-in analyzer to eliminate black-box factors during MPs measurements and to enable more accurate evaluation of measurement uncertainty. The FCM used in this study provides no accurate estimate of acquisition dead time; therefore, there is no reliable basis to quantify the reduction in particle number concentration caused by coincidence loss. In contrast, the custom-built analyzer records all information (*e.g.*, pulse width) required to calculate the probability of coincidence loss. This capability enables accurate estimation of the uncertainty associated with coincidence loss.

For FCM measurements, the SS and FL pulse heights of individual particles were recorded and visualized as a scatter plot (*e.g.*, *x*-axis: SS pulse height, *y*-axis: FL pulse height). A region of interest was defined within this scatter plot, and data within that region were extracted. This enabled the discrimination of target particles from others—a process commonly referred to as gating. The specific procedure was as follows. First, threshold voltages for the SS and FL signals were set based on the size of the target PS particles (details on how these threshold voltages were determined are described below). Using these thresholds, each particle was classified into one of three categories based on its SS and FL pulse heights: fluorescent particles (stained MPs), nonfluorescent particles (unstained MPs and impurities), and background noise. The specific classification criteria were as follows (see Fig. 2):

1. Particles with SS signal intensities below the SS threshold—regardless of FL intensity—were considered impurities or background noise and excluded from the count.

2. Particles exceeding the SS threshold but below the FL threshold were identified as nonfluorescent particles, which were either insufficiently stained MPs or impurities.

3. Particles exceeding both the SS and FL thresholds were identified as fluorescent particles stained by the swelling-mediated staining method, *i.e.*, MPs.

Table 1 summarizes the SS and FL threshold voltages for 2, 5, and 10 μm PS particles. It also lists the gain levels set for the photomultiplier tube (PMT) and the flow rates used during measurement. For example, in the case of 2 μm PS particles, the SS threshold was set to 380 mV, corresponding to the scattering intensity of 1 μm PS particles. Particles with SS voltages above 380 mV were counted as 2 μm PS particles. The FL threshold was set to 450 mV to ensure reliable detection of FL signals from 2 μm PS particles while excluding background noise. This value

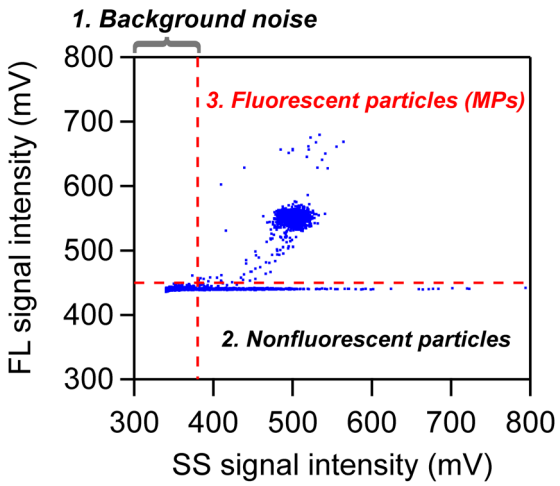

Fig. 2 Gating strategy for data analysis. Each blue dots represents a detected particle (event). The vertical and horizontal dashed lines represent the side-scatter (SS) and fluorescence (FL) thresholds, respectively. Events above both thresholds are classified as "3. Fluorescent particles"; Events above the SS threshold but below the FL threshold are classified as "2. Nonfluorescent particles"; all remaining events (below the SS threshold) are treated as "1. Background noise".

Table 1 FCM measurement configurations

PS particles	SS threshold	FL threshold	The PMT[a] gain for SS	The PMT gain for FL	Flow rate (μL s^{-1})
2 μm	380 mV[b]	450 mV	100	250	1
5 μm	476 mV[c]	550 mV	100	200	1
10 μm	476 mV[c]	550 mV	100	150	1

[a] PMT: photo multiplier tube. [b] Median pulse height voltage measured from 1 μm PS standard particles. [c] Median pulse height voltage measured from 2 μm PS standard particles.

was determined empirically based on the operator's experience. The signals from the PMT included offset voltages due to dark currents, typically around 330 mV for SS and 440 mV for FL. To minimize contamination from such noise, the threshold voltages were set slightly higher, as presented in Table 1.

2.4 Evaluation of staining efficiency, recovery rate, and counting efficiency

To assess the performance of the swelling-mediated staining method, the staining efficiency and recovery rate were evaluated using FCM. The staining efficiency (η_{stain}) is the ratio of the number concentration of MPs exhibiting FL to the total number concentration of MPs, as determined *via* SS signal analysis:

$$\eta_{stain} = \frac{C_{FL} - C_{FL,blank}}{C_{SS} - C_{SS,blank}} \quad (1)$$

where C_{FL} denotes the number concentration of fluorescent particles, $C_{FL,blank}$ is the number concentration of fluorescent particles in the blank sample, C_{SS} represents the total number concentration (based on SS signal), and $C_{SS,blank}$ indicates the number concentration of particles in the blank sample detected by SS. The staining efficiency represents the proportion of MPs stained with NR among the added MPs added.

The recovery rate ($\eta_{recovery}$) is defined as the ratio of the number concentration of fluorescent MPs to the number concentration of MPs originally added to the PS suspension, and is calculated as

$$\eta_{recovery} = \frac{C_{FL} - C_{FL,blank}}{C_{Ref}} \times DF \quad (2)$$

Here, C_{ref} denotes the number concentration of the PS standard suspension as determined by the M-OPC method, and DF indicates the dilution factor for each PS suspension. The recovery rate signifies the quantification performance of MPs when combining the swelling-mediated staining method with FCM measurement but not including up-front processes such as preconcentration and separation.

In addition to staining efficiency and recovery rate, the counting efficiency of the FCM was assessed by analyzing the SS signal. The counting efficiency (η_{count}) is defined as the ratio of the total number concentration obtained from FCM measurements to the reference number concentration of the PS standard suspension, and is calculated as follows:

$$\eta_{count} = \frac{C_{SS} - C_{SS,blank}}{C_{Ref}} \times DF. \quad (3)$$

Under ideal measurement conditions, the counting efficiency is equal to 1. However, various sources of uncertainty can cause deviation from this ideal value. For example, particle loss due to sedimentation or adsorption within the flow path (from the sample tube at the FCM inlet to the laser irradiation area in the flow cell), systematic errors in the sample flow rate, or particle coincidence events may significantly impact the counting efficiency.

Notably, the values of $C_{SS,blank}$ and $C_{FL,blank}$, obtained from blank samples, were negligibly small compared to the number concentration of the added PS particles (0.9×10^5 particles mL^{-1}), accounting to less than 0.8% of the total number concentration and less than 0.02% of the number concentration of fluorescent particles. Therefore, blank corrections were omitted in eqn (1)–(3) during the optimization experiments for the swelling-mediated staining method (Sections 3.1–3.3). In contrast, for the quantitative evaluation of staining efficiency (Sections 3.5–3.7), blank corrections were applied as defined in eqn (1)–(3).

Notably, the product of the staining efficiency (η_{stain}) and counting efficiency (η_{count}), as obtained from eqn (1) and (3), respectively, corresponds to the recovery rate ($\eta_{recovery} = \eta_{stain} \times \eta_{count}$).

3 Results and discussion

This chapter presents the findings of the optimization of the swelling-mediated staining method (Sections 3.1–3.3) and the performance evaluation using PS suspensions as test samples based on the optimized staining procedure (Sections 3.4–3.7). Specifically, Sections 3.1–3.3 delineate the optimization of the THF, NR, and Tween-20 concentrations, respectively. The outcomes of these optimizations were incorporated into the staining procedure discussed in Section 2.2. Based on this optimized procedure, the following results are presented: evaluation of FL intensity after swelling-mediated staining (Section 3.4), evaluation of particle number concentration dependence (Section 3.5), evaluation of particle size dependence (Section 3.6), and recovery tests using simulated environmental samples (Section 3.7). Here, "optimization" refers to tuning within limited sample sets. The optimized staining procedure developed here is tailored to specific environmental matrix and polymer type, with no claim to universal applicability across diverse matrices or polymers. We performed a series of univariate optimizations, which typically provide a local optimum rather than a global optimum. Nevertheless, the

staining efficiencies were sufficient to quantify MP number concentration. Therefore, our approach is a practical option for users applying the swelling-mediated staining method to their samples.

3.1 Optimization of the swelling-mediated staining procedure: THF concentration

To optimize the THF concentration in the swelling-mediated staining procedure, 2 μm PS suspensions were prepared with THF concentrations (v/v) of 5%, 10%, 15%, 20%, 25%, 30%, 40%, and 50%. The staining efficiency and counting efficiency, as determined by FCM, were compared. Here, the volume concentration refers to the THF concentration at the onset of evaporation, immediately after the addition of the NR solution. The NR solution and Tween-20 aqueous solution were added following the procedure presented in Section 2.2, with final NR and Tween-20 concentrations set at 10 μg mL^{-1} and 0.1%, respectively. Fig. 3 displays the staining and counting efficiencies at each THF concentration. No correction was applied using the number concentration of blank samples (see eqn (1) and (3)). At THF concentrations ≥15%, the staining efficiency remained nearly constant at approximately 1. Conversely, at concentrations <15%, the staining efficiency decreased significantly, falling below 0.1 at 5%.

This reduction in staining efficiency at low THF concentrations (<15%) was likely because of insufficient swelling of the PS particles, which may have hindered NR diffusion into the particle interiors, resulting in lower FL intensity. Conversely, the counting efficiency decreased at high THF concentrations (>30%), possibly due to irreversible changes caused by excessive swelling of the PS particles—such as partial dissolution in the solvent or fusion between swollen particles—that prevented the particles from returning to their original size after THF evaporation. Similar irreversible changes, including adsorption and fusion of MPs under high organic solvent concentrations, have also been reported in previous studies.[20] Based on the results presented in Fig. 3, both staining and counting efficiencies approached 1 (100%) within the THF concentration range of 15% to 30%. Therefore, a THF concentration of 25% was adopted for subsequent experiments.

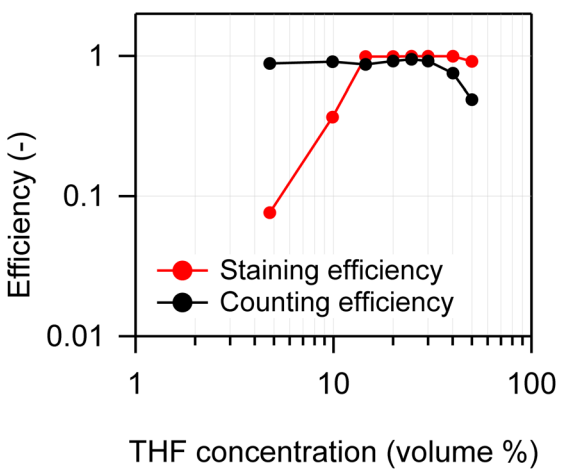

Fig. 3 Effect of THF concentration on the staining and counting efficiencies of 2 μm PS particles.

3.2 Optimization of the staining procedure: Nile red concentration

To optimize the NR concentration in the swelling-mediated staining procedure, 2 μm PS suspensions were prepared with NR mass concentrations of 1, 2, 5, 10, 20, 50, 100, 200, and 300 μg mL^{-1}. These values represent the final concentrations after removal of the organic solvent by evaporation. FL and scattered light intensities obtained by FCM, as well as staining and counting efficiencies, were compared across these concentrations. THF and Tween-20 aqueous solutions were added according to the procedure described in Section 2.2, with the THF concentration adjusted to 25% and the Tween-20 concentration set at 0.1%. The staining efficiency, counting efficiency, the modal FL signal intensity, and 1-D histograms of FL signal intensity at each NR concentration are displayed in Fig. 4(a)–(c). Here, FL intensity refers to the most frequent voltage value in the pulse height distribution of the FL signal. No correction was applied using the number concentration of blank samples (see eqn (1) and (3)). At NR concentrations ≤50 μg mL^{-1}, both staining and counting efficiencies remained nearly constant at approximately 1. Conversely, at NR concentrations ≥100 μg mL^{-1}, staining and counting efficiencies exhibited substantial fluctuations in opposite directions (Fig. 4(a)). Regarding FL intensity (Fig. 4(b) and (c)), the maximum value (approximately 530 mV) was observed when the NR concentration was between 5 and 10 μg mL^{-1}.

At high NR concentrations (>100 μg mL^{-1}), the apparent fluctuations in staining and counting efficiencies were artifacts caused by the formation of NR aggregates rather than actual changes in staining performance. Previous studies have indicated that most NR aggregates are smaller than approximately 1 μm.[17,26] In this study, the side-scatter (SS) signal detected NR aggregates up to approximately 2 μm in size, overlapping with the signal peak corresponding to PS particles. As a result, the total particle number concentration (C_{SS}) increased when the NR concentration exceeded 200 μg mL^{-1}. In aqueous media, NR molecules aggregate *via* π–π stacking to form H-aggregates,[30–32] a state known to strongly reduce transition probability and promote nonradiative decay (aggregate-induced quenching);[33] therefore, NR aggregates exhibit no fluorescence.[17,26] Accordingly, the number concentration of fluorescent particles measured by FCM (C_{FL}) remained constant or decreased, while C_{SS} increased. Therefore, the apparent inverse variation in counting and staining efficiencies observed in Fig. 4(a) can be attributed to this phenomenon. The asymmetry in counting and staining efficiencies resulted from inconsistent variations in C_{SS} and the C_{FL}. A detailed analysis of the underlying mechanism is beyond the scope of this study. As shown in Fig. 4(b), the modal FL intensity peaked at NR concentrations between 5 and 10 μg mL^{-1}, and then decreased with increasing NR concentration. At NR concentrations below 5 μg mL^{-1}, the modal FL intensity declined, likely due to a reduced amount of NR encapsulated

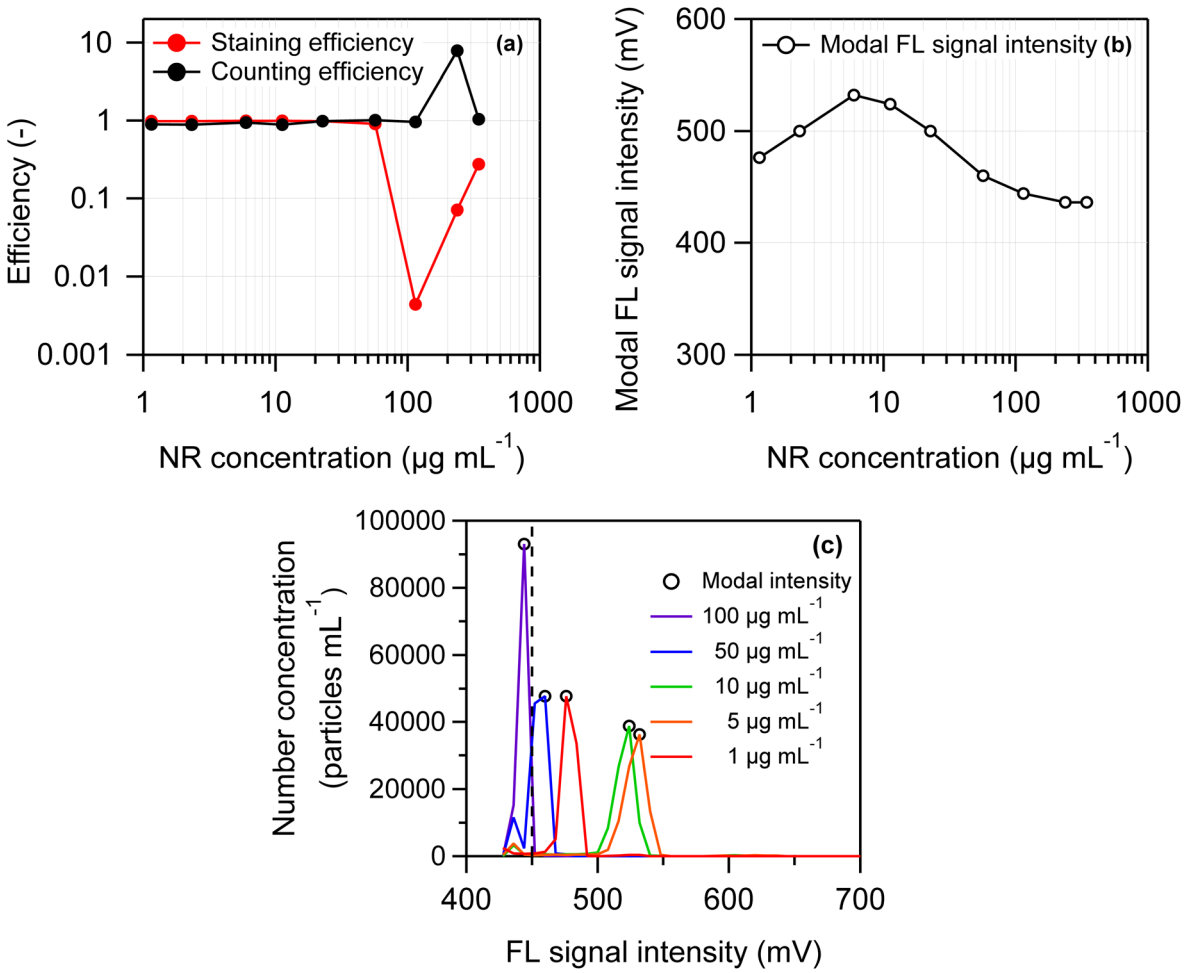

Fig. 4 Effect of Nile red (NR) concentration on the staining and counting efficiencies, and fluorescence intensity of 2 μm PS particles. (a) The staining and counting efficiencies, (b) the modal fluorescence (FL) signal intensity, (c) the overlaid FL histograms. For clarity, only selected data are shown in (c). Open circles in panel (c) indicate the peaks of each fluorescence signal distribution, with their *x*-axis values representing the modal FL signal intensity for each NR concentration shown in panel (b). The vertical dashed line in (c) denotes the FL threshold for 2 μm PS particles (450 mV).

per particle. A similar decrease in the modal FL intensity was observed at higher concentrations (>20 μg mL^{-1}), likely due to the formation of NR aggregates. As previously mentioned, NR forms nonfluorescent aggregates, and higher NR concentrations are expected to result in a greater proportion of these aggregates within the stained PS particles. Consequently, the FL intensity may decrease. Summarizing the results shown in Fig. 4(a)–(c), both staining and counting efficiency approached approximately 1 (100%) within the NR concentration range of 1–50 μg mL^{-1}. Based on these findings, an NR concentration of 10 μg mL^{-1}, which maximizes FL intensity per particle, was adopted for subsequent experiments.

3.3 Optimization of the staining procedure: Tween-20 concentration

To optimize the concentration of Tween-20 during the swelling-mediated staining procedure, a series of 2 μm PS suspensions were prepared with varying volume concentrations (v/v) of Tween-20: 0.001%, 0.005%, 0.01%, 0.05%, 0.1%, 0.5%, and 1%. The staining and counting efficiencies obtained from FCM measurements were compared across these concentrations. Here, the volume concentration refers to the value after the sample was diluted 11-fold with ultrapure water following the evaporation of THF. THF and NR solution were added according to the procedure described in Section 2.2, with final concentrations adjusted to 25% for THF and 10 μg mL^{-1} for NR. The staining and counting efficiencies at each Tween-20 concentration are illustrated in Fig. 5. No correction using the number concentration of blank samples (see eqn (1) and (3)) was applied. For the Tween-20 concentration at ≥0.05%, both staining and counting efficiencies remained nearly constant at approximately 1. Conversely, for concentrations at ≤0.01%, the efficiencies demonstrated significant fluctuations.

At Tween-20 concentrations at or below 0.01%, the staining efficiency appeared to decrease from 1, while the counting efficiency appeared to increase—possibly due to NR aggregation caused by reduced surface activity of Tween-20, rather than actual changes in efficiency. NR is a hydrophobic dye that

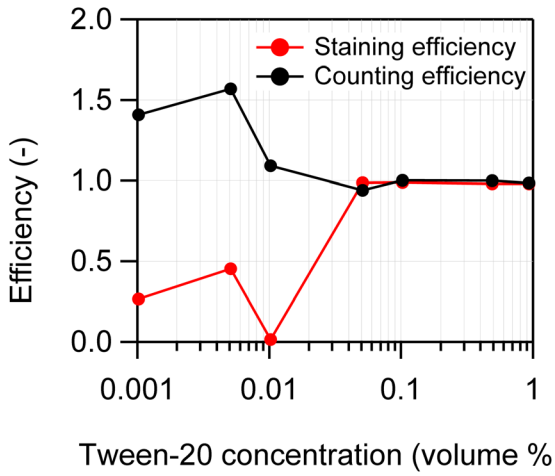

Fig. 5 Effect of Tween-20 concentration on the staining and counting efficiencies of 2 μm PS particles.

readily aggregates in aqueous media lacking surfactants.[17,32] As described in Section 3.2, NR aggregates emit no FL. The number concentration of fluorescent particles remained constant or decreased, whereas the total particle number concentration increased. Consequently, these observations explain the apparent opposite trends in counting and staining efficiencies shown in Fig. 5. The asymmetry in these efficiencies resulted from inconsistent variations in C_{SS} and the C_{FL}, as discussed in Section 3.2. Summarizing the results shown in Fig. 5, both staining and counting efficiencies approached nearly 1 (100%) within the Tween-20 concentration range of 0.05% to 1%. Based on these results, a Tween-20 concentration of 0.1% was adopted for subsequent experiments, as higher surfactant concentrations increase the risk of bubble formation.

3.4 Performance evaluation: comparison between the swelling and nonswelling staining methods

To assess the fluorescent staining performance of the swelling-mediated method, we visually compared PS suspension samples with and without the staining treatment. Fig. 6 presents fluorescence microscope images of 10 μm PS particles stained with and without prior swelling. Fig. 6(a) and (b) present the bright-field and dark-field FL images, respectively, taken from the same field of view. For dark-field FL imaging, a mercury lamp was used as the light source. An excitation filter of 400–440 nm and an emission filter transmitting wavelengths above 475 nm were used to capture the particle images. The stained particles with swelling (denoted as "Swelling") were prepared following the procedure described in Section 2.2. The stained particles without swelling (denoted as "No swelling") were prepared using the same procedure, except that ethanol—a poor solvent for PS—was used in place of THF, thereby preventing particle swelling during staining. As presented in Fig. 6(a) and (b), the FL intensity of swollen and nonswollen particles, observed under identical conditions, differed markedly, with the THF-swollen PS particles exhibiting substantially stronger FL. These results show that the swelling-mediated staining method is a highly effective fluorescent staining technique.

3.5 Performance evaluation: dependency on particle number concentration

The applicability of the swelling-mediated staining method described in Section 2.2 was assessed across various particle number concentrations. Test samples containing 2 μm PS suspensions were prepared by varying the volume of the PS standard suspension added to the vials, resulting in concentrations ranging from 1000 particles mL^{-1} to 100 000 particles mL^{-1}. The FCM results for each concentration, along with the corresponding staining and counting efficiencies, are displayed in Fig. 7(a) and (b), respectively. According to eqn (1) and (3), the FCM-derived number concentrations of fluorescent and total particles were corrected by subtracting the values obtained from blank samples. The horizontal axis labeled "Reference concentration" denotes the particle number concentration of the PS standard suspension, determined using the M-OPC method and adjusted for the dilution factor. As presented in Fig. 7(a),

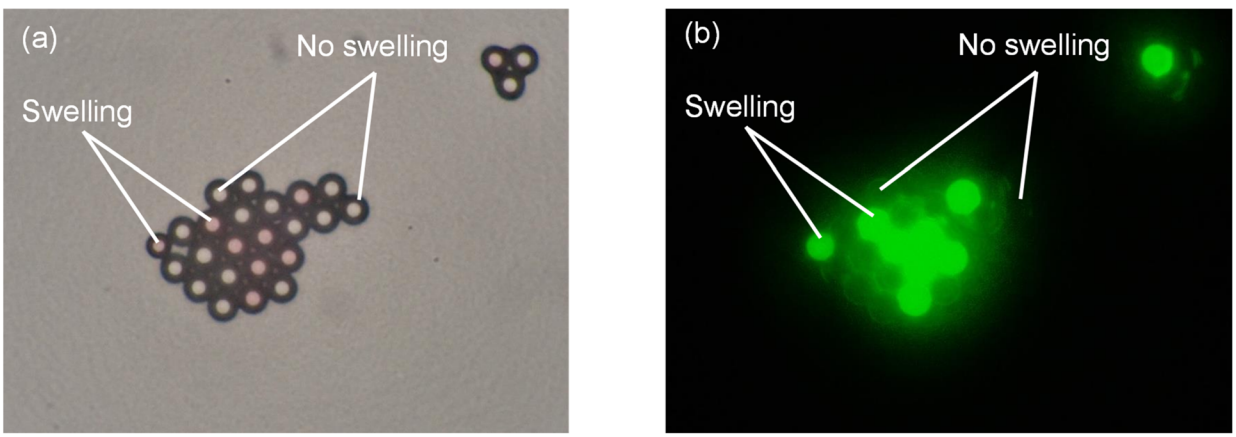

Fig. 6 Fluorescence microscope images of a mixture of 10 μm PS particles stained with and without prior swelling. (a) Bright field image, (b) dark field fluorescence image.

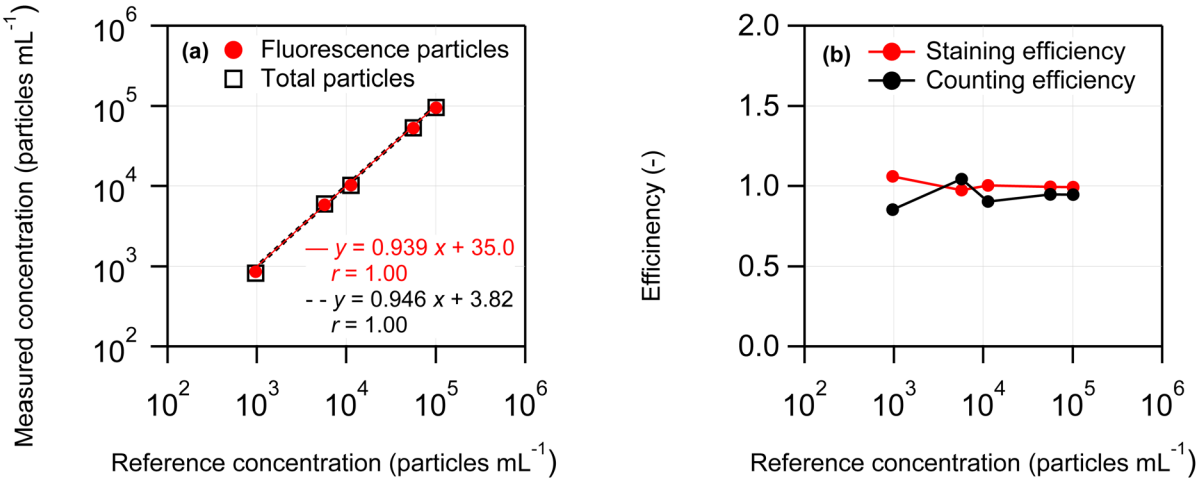

Fig. 7 Effect of particle number concentration (2 μm PS particles) on the swelling-mediated staining technique. (a) Reference concentration *versus* measured concentration for fluorescent particles and total particles. (b) Reference concentration *versus* staining and counting efficiencies.

the particle number concentration obtained by FCM exhibited a positive linear correlation with the reference concentration. Furthermore, as illustrated in Fig. 7(b), both staining and counting efficiencies remained close to 1 across the entire concentration range tested. These findings show the effectiveness of the swelling-mediated staining method within the range of 1000 particles mL^{-1} to 100 000 particles mL^{-1}. Additionally, the FL and scattered light intensities of individual PS particles were unaffected by the particle number concentration and remained stable (data not shown).

The applicable concentration range is more strongly influenced by the counting performance of FCM than by the staining method itself. For low-concentration samples, the particle counts measured by FCM decrease, leading to greater variability and reduced statistical reliability. For example, at the lowest tested concentration (1000 particles mL^{-1}), the total particle count from three repeated measurements was approximately 100 particles, and this variability became the primary source of measurement uncertainty. For environmental samples containing low number concentrations of MPs, either preconcentration prior to swelling-mediated staining or an increase in the sample volume per FCM measurement is required. There is no widely accepted standard protocol for preconcentration of MPs smaller than 100 μm, and it remains a common challenge across many measurement techniques, including FCM. Preconcentration is outside the scope of this study; no further discussion is provided.

At high FCM concentrations, coincidence loss can become a primary source of measurement uncertainty. Coincidence loss reduces the apparent particle count, leading to an underestimation of the MP number concentration. The rate of coincidence loss depends on particle number concentration, flow rate, and sensor dead time.[34,35] To analyze environmental samples with high MP number concentration, dilution to the optimal concentration range is necessary. Alternatively, the measured number concentration can be corrected using the calculated coincidence loss rate. At the highest particle number concentration tested in this study (1×10^5 particles mL^{-1}; see Fig. 7), the coincidence loss rate was approximately 0.1%, indicating a negligible influence on the measured concentration.

In conclusion, the swelling-mediated staining method was shown to be an effective FL staining technique across the particle number concentration range suitable for FCM measurements.

3.6 Performance evaluation: dependency on particle size

The swelling-mediated staining method was validated using PS standard suspensions with particle sizes of 2, 5, and 10 μm. As described in Section 3.5, PS standard suspensions with a particle number concentration of 1×10^6 particles mL^{-1} were used. After staining and dilution, the particle number concentration was 0.9×10^5 particles mL^{-1}. The staining efficiency and recovery rate for each particle size are presented in Fig. 8(a) and (b), respectively. Table 2 summarizes the staining efficiency, recovery rate, counting efficiency, and associated uncertainties. The FL and total particle number concentrations measured by FCM were corrected using the blank sample concentrations, as described in eqn (1) and (2). The error bars on the vertical axis represent the expanded uncertainties at a level of confidence of 95%. The measurement uncertainties were evaluated in accordance with the Guide to the Expression of Uncertainty in Measurement (GUM).[36] Applying the law of propagation of uncertainty to eqn (1)–(3) yielded combined standard uncertainties for the staining efficiency, recovery rate, and counting efficiency, respectively. Expanded uncertainties were calculated by multiplying a coverage factor $k = 2$. The uncertainty in staining efficiency includes contributions from repeatability, between-vial variation, and coincidence loss for both the FL particle number concentration C_{FL} and the total particle number concentration C_{SS}. Likewise, the uncertainty in the recovery rate includes contributions from repeatability,

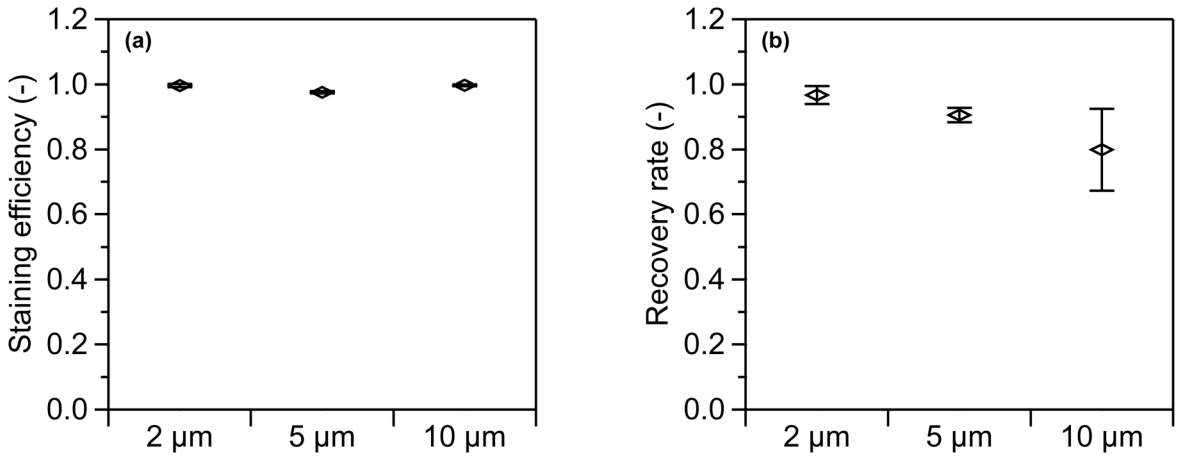

Fig. 8 Effect of particle size on the swelling-mediated staining technique. (a) Staining efficiencies and (b) recovery rates for 2 μm, 5 μm, and 10 μm PS particle suspensions. Error bar represents expanded uncertainty. A coverage factor of $k = 2$ was used for an approximate level of confidence level of 95%.

Table 2 Summary of FCM measurement results for 2, 5, and 10 μm PS particle suspensions

PS particle suspension	Staining efficiency	Recovery rate	Counting efficiency
2 μm	0.996 ± 0.005^a	0.968 ± 0.028^a	0.972 ± 0.026^a
5 μm	0.976 ± 0.003^a	0.906 ± 0.022^a	0.928 ± 0.024^a
10 μm	0.997 ± 0.003^a	0.799 ± 0.126^a	0.801 ± 0.127^a

[a] Expanded uncertainty with a coverage factor of $k = 2$ (a level of confidence of 95%).

between-vial variation, coincidence loss for C_{FL}, and the uncertainty of the reference concentration. As presented in Fig. 8(a), the staining efficiency was close to 1 for all particle sizes. According to Fig. 8(b), the recovery rate depended on particle size, decreasing as particle size increased. For the 10 μm PS suspension, the recovery rate dropped to as low as 0.8 and exhibited the largest uncertainty. Component-wise contributions were quantified using the coefficient of contribution,[37] defined for mutually uncorrelated inputs as $h(y,x_i) = [c_i u(x_i)/u_c(y)]^2$, where c_i is the sensitivity coefficient, $u(x_i)$ is the standard uncertainty of x_i, and $u_c(y)$ is the combined standard uncertainty. The $h(y,x_i)$ is dimensionless and sum to 1 (100%). Using this metric, repeatability and between-vial variation together accounted for 99% of $u_c(y)$ for the 10 μm PS suspension.

The results presented in Fig. 8(a) show that the swelling-mediated staining method is effective across the tested particle size range (2–10 μm). The staining efficiency—defined as the ratio of the fluorescent particle number concentration to the total particle number concentration (eqn (1))—was approximately 1. This indicates that nearly all MPs added during the swelling-mediated staining process were successfully stained with NR. Furthermore, the uncertainty associated with the staining efficiency was less than 0.006 (<0.5%), indicating that the measurement results were highly reliable.

Fig. 8(b) shows the presence of a size-dependent factor that introduced a systematic bias in the recovery rate. One possible explanation is the reduced counting efficiency of FCM for larger particle sizes. A comparison between the recovery rates and counting efficiencies presented in Table 2 shows that these values are consistent within the uncertainty range. This suggests that the reduced recovery rate may be the primary cause of the low counting efficiency. For environmental samples, an accurate number concentration of MPs can be obtained by correcting the measured values using the corresponding counting efficiency.

Gravitational settling contributes to the decrease in counting efficiency. This is consistent with the observation that larger particles, which have higher gravitational settling velocities, exhibit a more pronounced reduction in counting efficiency. However, complete settling of 10 μm PS particles to the bottom of a test tube (approximately 5 cm in length) positioned at the FCM inlet takes several hours. As each FCM measurement was completed within 5 min of sample transfer, factors other than gravitational settling must also contribute to the observed particle loss.

Another likely reason is particle adsorption onto the inner walls of the flow path or flow cell in the FCM, or clogging within these components. To minimize such adsorption and clogging, the flow rate for FCM measurements was increased from 1 μL s^{-1} to 3 μL s^{-1}, which improved the counting efficiency to over 0.95 (data not shown). This finding indicates that particle adsorption and clogging are likely major contributors to the reduced efficiency. As contamination within the flow path was suspected to cause significant particle adsorption, thorough cleaning was performed before and after each FCM measurement. Despite these efforts, the counting efficiency remained unchanged. Replacing the tubing connecting the test tube to the flow cell was considered a potentially effective validation method. However, this approach could not be implemented due to the difficulty of accessing the FCM interior and associated risk of laser misalignment.

To explore differences in adsorption characteristics between samples measured using the swelling-mediated staining

method and those measured without it, unstained PS particles were measured using FCM. The results showed that, similar to the swelling-mediated stained samples, the counting efficiency exhibited a decreasing trend with increasing particle size. This finding shows that the decrease in counting efficiency stems from the intrinsic counting performance of the FCM rather than from the swelling-mediated staining of MPs. Further detailed investigations into the factors contributing to reduced counting efficiency for larger particle sizes, as well as potential improvements, remain subjects for future research. Notably, the FCM employed in this study was a modified version, with flow channel components differing from those of commercial instruments, which may affect the reproducibility of this phenomenon.

3.7 Performance evaluation: recovery rate of simulated environmental samples

A recovery test using simulated environmental samples was conducted to assess the validity of the swelling-mediated staining method. The environmental samples consisted of a mixture of tap water and kaolin particles. Recovery rates were evaluated for 2, 5, and 10 μm PS standard suspensions spiked into the mixture. After staining and dilution, the particle number concentration was 0.4×10^5 particles mL^{-1}. The fluorescent and total particle number concentrations measured by FCM were corrected by subtracting the particle number concentration of the blank samples, as described in eqn (2). In addition to the recovery rate defined in eqn (2), a corrected recovery rate was also calculated by dividing the recovery rate by the FCM counting efficiency shown in Table 2.

The recovery rates for each particle size, along with the recovery rates corrected for counting efficiencies, are presented in Fig. 9(a) and (b), respectively. The error bars on the vertical axis represent the expanded uncertainties at a level of confidence of 95%. The uncertainty in the recovery rate includes contributions from the repeatability of the fluorescent particle number concentration (C_{FL}), between-vial variation, coincidence loss, and uncertainty in the reference concentration. The uncertainty in the corrected recovery rate includes these factors as well as the uncertainty in the counting efficiency. As illustrated in Fig. 9(a), the recovery rates and their expanded uncertainties for the 2, 5, and 10 μm PS suspensions were 0.965 ± 0.030, 0.917 ± 0.022, and 0.678 ± 0.079, respectively. Consistent with the trend observed in Fig. 8(b), the recovery rates exhibit a size-dependent trend, with lower values corresponding to larger particle sizes. Specifically, the recovery rate for 10 μm PS suspension was 0.678, accompanied by the largest uncertainty. The primary sources of uncertainty for the 10 μm PS suspension were repeatability and between-vial variation, which together accounted for 97% of the combined standard uncertainty. As presented in Fig. 9(b), the corrected recovery rates and their expanded uncertainties for the 2, 5, and 10 μm PS suspensions were 0.993 ± 0.038, 0.988 ± 0.029, and 0.846 ± 0.100, respectively. Correction for counting efficiency increased the recovery rates for all particle sizes, bringing them closer to 1 compared to Fig. 9(a). In particular, the values for the 2 and 5 μm PS suspensions agreed with 1.0 within the range of uncertainty. These results demonstrate that the PS standard suspensions added to the simulated environmental samples were effectively recovered. For the 10 μm PS suspension, the correction yielded a recovery rate of 0.846, reflecting a moderate shortfall in the correction.

The results presented in Fig. 9(a) suggest that the measurement outcomes for the simulated environmental samples were consistent with those obtained using the ultrapure water medium (see Section 3.6). Both sample types exhibited a particle size dependence in the recovery rate, with the lowest value observed for the 10 μm PS suspensions. The combined standard uncertainties were also comparable between the samples, and the measurement uncertainty was primarily dominated by repeatability and between-vial variation. These findings show that, at least for the 2 and 5 μm PS suspensions, no significant sources of uncertainty would lead to

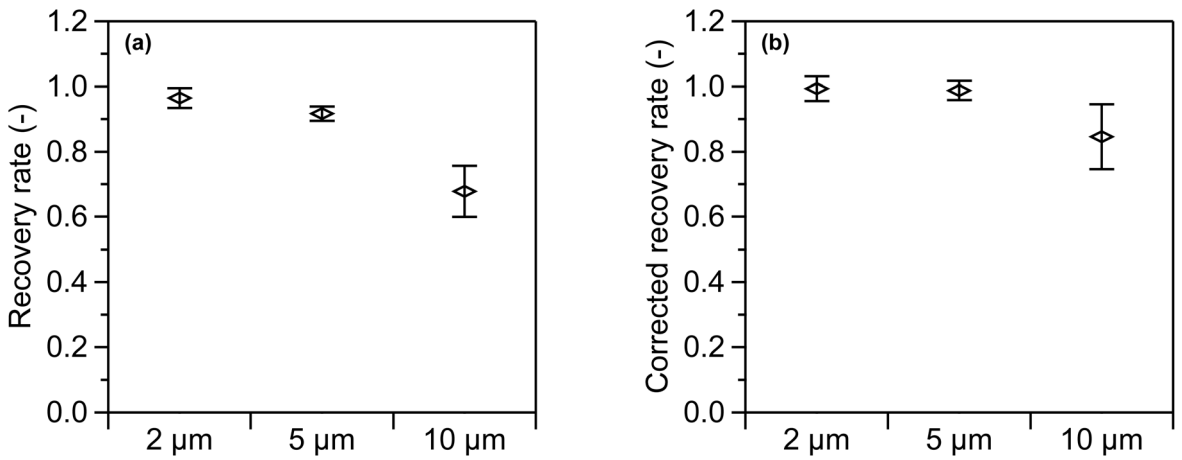

Fig. 9 Recovery test of simulated environmental samples with 2 μm, 5 μm, and 10 μm PS particles. (a) Recovery rates and (b) corrected recovery rates for 2 μm, 5 μm, and 10 μm PS particle suspensions. The error bars represent the expanded uncertainty. A coverage factor of $k = 2$ was adopted for an approximate level of confidence of 95%.

discrepancies between the results obtained using the ultrapure water and the simulated environmental matrices.

The corrected recovery rates shown in Fig. 9(b) show that accurate quantification of MP number concentrations was achieved for the 2 and 5 μm PS suspensions, as they were successfully corrected using the counting efficiencies. Conversely, the corrected recovery rate for the 10 μm PS suspension remained below 1, highlighting a deviation from full recovery. This outcome was likely due to the limited reproducibility of the FCM counting efficiency. Particle adsorption, described in Section 3.6 as one of the major sources of uncertainty, appears to have contributed to this outcome. Because adsorption depends on the surface condition of the internal flow path in the FCM, it can behave inconsistently. Indeed, substantial day-to-day variations in counting efficiency were observed, and even same-day measurements occasionally produced inconsistent results. Gaining insight into the origin of this variation and implementing countermeasures is critical in achieving accurate quantification of MP number concentrations. Although some sources of uncertainty affecting the 10 μm PS suspension remain to be identified, the observation that the corrected recovery rate exceeded 0.8 is significant and supports the potential for reliable quantification. Thus, this degree of accuracy denotes a viable level for screening applications requiring semiquantitative assessments.

Summarizing the above findings, we demonstrated that the swelling-mediated staining method is effective even for samples containing trace amounts of non-MPs impurities. MP samples collected from the environment typically contain various inorganic and organic substances, as well as impurity particles, depending on the sampling location. The experiments conducted in this study represent validation tests under controlled and limited conditions. In MP analysis of marine, river, soil, or atmospheric samples, pretreatment steps such as organic matter decomposition and density separation are typically performed to remove impurities. These pretreatment processes are generally similar across different types of environmental samples. Thus, swelling-mediated staining is expected to be effective for such pretreated samples; however, the staining protocol requires optimization for individual sample matrices and polymer types. The performance evaluation presented in this study serves as a preliminary assessment of the practical application of the swelling-mediated staining method across various environmental matrices. Future studies applying this method to MPs of mixed sizes and different polymer types, including potentially weathered MPs in environmental samples, will advance rapid MPs quantification using FCM. Furthermore, the observed size-dependent variations in counting efficiency reflect the inherent performance characteristics of the FCM used, rather than systematic uncertainties associated with the swelling-mediated staining method.

4 Conclusions

In this study, we demonstrated the rapid quantification of MP number concentrations by optimizing a highly efficient staining method based on the swelling technique for FCM measurements. This method uses the swelling behavior of polymers in organic solvents to stain the interior of MPs. The staining efficiency of micrometer-sized PS particles was nearly 1.0 (100%), and these stained particles exhibited significantly higher fluorescence intensity under fluorescence microscopy than those prepared by conventional methods, in which NR is merely adsorbed onto the particle surface. We also confirmed that staining is feasible for environmental samples containing trace amounts of non-MPs impurities. In addition, counting efficiency, recovery rate, and associated measurement uncertainties were accurately determined using standard suspensions with precisely determined particle number concentrations. The recovery rates obtained from FCM measurements exhibited a size-dependent trend, with larger particles tending to have lower recovery rates, primarily due to decreased counting efficiency in FCM. Nevertheless, MP number concentrations could be accurately quantified by correcting the measurement results based on the counting efficiencies. The applicability of this method to polymers other than PS remains a subject for future research. This method is simple and cost-effective, requiring only inexpensive reagents. We anticipate that combining the swelling-mediated staining method and FCM will enable high-throughput quantitative assessment of MPs, particularly "missing plastics"[16,38,39] in the environment.

Author contributions

The manuscript was written with contributions from all authors. All authors have reviewed and approved the final version of the manuscript.

Conflicts of interest

The authors declare no conflict of interest.

Data availability

The data supporting this article have been included as part of the supporting information (SI). Supplementary information is available. See DOI: **https://doi.org/10.1039/d5ay01093d**.

Acknowledgements

This work was supported by the JSPS KAKENHI Grant Number JP24K15333 and Keio Leading-edge Laboratory of Science and Technology Research Grant for the Ph. D. program.

References

1 World Health Organization (WHO), *Dietary and Inhalation Exposure to Nano- and Microplastic Particles and Potential Implications for Human Health, Report 9789240054608*, World Health Organization, Geneva, 2022.
2 Y. Li, L. Tao, Q. Wang, F. Wang, G. Li and M. Song, *Environ. Health*, 2023, **1**, 249–257.

3 The European Chemicals Agency (ECHA), Committee for Risk Assessment (RAC) Committee for Socio-economic Analysis (SEAC) Background Document to the Opinion on the Annex XV report proposing restrictions on intentionally added microplastics, 2020, https://echa.europa.eu/documents/10162/b56c6c7e-02fb-68a4-da69-0bcbd504212b, 31 March, 2025 accessed.
4 S. Zhao, K. F. Kvale, L. Zhu, E. R. Zettler, M. Egger, T. J. Mincer, L. A. Amaral-Zettler, L. Lebreton, H. Niemann, R. Nakajima, M. Thiel, R. P. Bos, L. Galgani and A. Stubbins, *Nature*, 2025, **641**, 51–61.
5 C. Cai, L. Zhu and B. Hong, *Mar. Pollut. Bull.*, 2023, **193**, 115136.
6 A. González-Acedo, E. García-Recio, R. Illescas-Montes, J. Ramos-Torrecillas, L. Melguizo-Rodríguez and V. J. Costela-Ruiz, *Chemosphere*, 2021, **280**, 130826.
7 Z. Liu and X.-y. You, *Sci. Total Environ.*, 2023, **903**, 166766.
8 Y. Michida, S. Chavanich, S. Chiba, M. R. Cordova, A. Cozsar Cabanas, F. Galgani, P. Hagmann, H. Hinata, A. Isobe, P. Kershaw, N. Kozlovskii, D. Li, A. L. Lusher, E. Marti, S. A. Mason, J. Mu, H. Saito, W. J. Shim, A. D. Syakti, H. Takada, R. Thompson, T. Tokai, K. Uchida, K. Vasilenko and J. Wang, *Guidelines for Harmonizing Ocean Surface Microplastic Monitoring Methods*. Version 1.2., Chiyoda-ku, Tokyo, Japan, 2023.
9 J. Masura, J. Baker, G. Foster and C. Arthur, Laboratory methods for the analysis of microplastics in the marine environment: recommendations for quantifying synthetic particles in waters and sediments, *NOAA Marine Debris Division*, Siver Spring, MD, 2015.
10 C. Schwaferts, R. Niessner, M. Elsner and N. P. Ivleva, *Trends Anal. Chem.*, 2019, **112**, 52–65.
11 S. Belz, I. Bianchi, C. Cella, H. Emteborg, F. Fumagalli, O. Geiss, D. Gilliland, A. Held, U. Jakobsson, R. La Spina, D. Méhn, Y. Ramaye, P. Robouch, J. Seghers, B. Sokull-Klüttgen, E. Stefaniak and J. Stroka, *Current Status of the Quantification of Microplastics in Water - Results of a JRC/BAM Inter-laboratory Comparison Study on PET in Water*, Report 978-92-76-40957-1, Publications Office of the European Union, Luxembourg, 2021.
12 F. Caputo, R. Vogel, J. Savage, G. Vella, A. Law, G. Della Camera, G. Hannon, B. Peacock, D. Mehn, J. Ponti, O. Geiss, D. Aubert, A. Prina-Mello and L. Calzolai, *J. Colloid Interface Sci.*, 2021, **588**, 401–417.
13 N. Kaile, M. Lindivat, J. Elio, G. Thuestad, Q. G. Crowley and I. A. Hoell, *Front. Mar. Sci.*, 2020, **7**, 12.
14 L. Ainé, J. Jacquin, C. Breysse, C. Colin, J.-M. Andanson and F. Delor-Jestin, *MethodsX*, 2025, **14**, 103200.
15 T. Maes, R. Jessop, N. Wellner, K. Haupt and A. G. Mayes, *Sci. Rep.*, 2017, **7**, 44501.
16 G. Erni-Cassola, M. I. Gibson, R. C. Thompson and J. A. Christie-Oleza, *Environ. Sci. Technol.*, 2017, **51**, 13641–13648.
17 A. Bianco, L. Carena, N. Peitsaro, F. Sordello, D. Vione and M. Passananti, *Environ. Chem. Lett.*, 2023, **21**, 647–653.
18 H. Zhu and M. J. McShane, *J. Am. Chem. Soc.*, 2005, **127**, 13448–13449.
19 Q. Zhang, Y. Han, W.-C. Wang, L. Zhang and J. Chang, *Eur. Polym. J.*, 2009, **45**, 550–556.
20 J.-H. Lee, I. J. Gomez, V. B. Sitterle and J. C. Meredith, *J. Colloid Interface Sci.*, 2011, **363**, 137–144.
21 T. Behnke, C. Würth, K. Hoffmann, M. Hübner, U. Panne and U. Resch-Genger, *J. Fluoresc.*, 2011, **21**, 937–944.
22 M. Pellach and S. Margel, *Chem. Cent. J.*, 2011, **5**, 6.
23 M. Pellach and S. Margel, *Photochem. Photobiol.*, 2014, **90**, 952–956.
24 W. S. Lee, H. Kim, Y. Sim, T. Kang and J. Jeong, *ACS Omega*, 2022, **7**, 2467–2473.
25 T. Behnke, C. Würth, E.-M. Laux, K. Hoffmann and U. Resch-Genger, *Dyes Pigm.*, 2012, **94**, 247–257.
26 Y.-T. Tse, H.-S. Lo, S. M. Chan and E. T. Sze, *Water*, 2022, **14**, 18.
27 Y. Kuruma, T. Sakaguchi and H. Sakurai, *Adv. Powder Technol.*, 2020, **31**, 848–858.
28 Y. Kuruma, T. Sakaguchi and H. Sakurai, *Metrologia*, 2021, **58**, 045007.
29 Japanese Industrial Standards Committee, JIS K 0101 — Testing methods for industrial water, 2017.
30 I. N. Kurniasih, H. Liang, P. C. Mohr, G. Khot, J. P. Rabe and A. Mohr, *Langmuir*, 2015, **31**, 2639–2648.
31 T. Felbeck, T. Behnke, K. Hoffmann, M. Grabolle, M. M. Lezhnina, U. H. Kynast and U. Resch-Genger, *Langmuir*, 2013, **29**, 11489–11497.
32 A. Ray, S. Das and N. Chattopadhyay, *ACS Omega*, 2019, **4**, 15–24.
33 S. Ma, S. Du, G. Pan, S. Dai, B. Xu and W. Tian, *Aggregate*, 2021, **2**, e96.
34 International Organization for Standardization, ISO 21501-2: Determination of particle size distribution — Single particle light interaction methods — Part 2: Light scattering liquid-borne particle counter, 2019.
35 International Organization for Standardization, ISO 21501-3: Determination of particle size distribution — Single particle light interaction methods — Part 3: Light extinction liquid-borne particle counter, 2019.
36 Joint Committee for Guides in Metrology (JCGM), Evaluation of Measurement Data –Guide to the Expression of Uncertainty in Measurement, 2008, DOI: 10.59161/jcgm100-2008e.
37 R. Kessel, R. Kacker and M. Berglund, *Metrologia*, 2006, **43**, S189.
38 M. Eriksen, M. Thiel and L. Lebreton, in *Hazardous Chemicals Associated with Plastics in the Marine Environment*, ed. H. Takada and H. K. Karapanagioti, Springer International Publishing, Cham, 2019, pp. 135–162, DOI: 10.1007/698_2016_123.
39 A. Isobe and S. Iwasaki, *Sci. Total Environ.*, 2022, **825**, 153935.